



Supplementary Materials for  
**A designed supramolecular protein assembly with in vivo enzymatic activity**

Woon Ju Song and F. Akif Tezcan\*

\*Corresponding author. E-mail: [tezcan@ucsd.edu](mailto:tezcan@ucsd.edu)

Published 19 December 2014, *Science* **346**, 1525 (2014)

DOI: 10.1126/science.1259680

**This PDF file includes:**

Materials and Methods  
Figs. S1 to S17  
Tables S1 to S5  
References

## Materials and Methods

**Protein Preparation.** PCR-based site-directed mutagenesis of the *cyt cb<sub>562</sub>* variants (Tables S1-S2) was carried out as previously published (23). The “triad” mutations to introduce Zn binding residues were made using the parent plasmid pET20b(+)<sup>C96</sup>RIDC1. The sequences of the primers used for the triad mutations are listed in Table S2. After mutagenesis, the plasmids were transformed into competent XL1-Blue or DH5 $\alpha$  *E. coli* cells. For sequencing, a single colony grown in LB/agar plates with 100 mg/L ampicillin was picked and grown in 5 mL LB media with 100 mg/L ampicillin for ~8 hrs at 37 °C. The plasmid was extracted using the Miniprep kit (5 Prime or Qiagen) and sequenced (Retrogen). The sequenced plasmid was transformed into competent BL21(DE3) *E. coli* cells which contained the *ccm* (cytochrome c maturation) cassette (36). The colonies were grown overnight at 37 °C on agar/LB plates containing 100 mg/L ampicillin and 30 mg/L chloramphenicol. Starter cultures were grown from single colonies from LB/agar plates in LB media containing the same amounts of antibiotics. After the cell growth at 37 °C for ~5-8 hrs, when OD<sub>600</sub> reached ~0.7-0.8, the cell culture was inoculated into 12-14 L of LB media. Proteins were expressed by autoinduction, whereby the cells were grown for ~16-20 hrs without the addition of IPTG. Protein purification was performed by standard procedures as described previously (23). Briefly, the protein was lysed by repeated cycles of sonication in 10 mM sodium phosphate buffer in an ice bath. The pH of the lysate was lowered to 5 to precipitate proteins other than *cb<sub>562</sub>* variants. After centrifugation and adjusting the pH to 8, the supernatant was loaded onto a Q sepharose column and eluted using a step-gradient in the range of 0-1 M NaCl in 10 mM NaPi, pH 8.0 buffer at 22 °C. After this step, the protein was further purified by on a high Q-cartridge column using a Biologic DuoFlow workstation (BioRad) using a linear gradient of 0-0.5M NaCl in 10 mM NaPi, pH 8.0 buffer. This step was followed by size exclusion chromatography on a Superdex 75 column using a buffer solution containing 20 mM Tris/HCl (pH 7.0) and 150 mM NaCl after reducing the protein with excess dithiothreitol (DTT). The purity of the protein was confirmed by SDS-PAGE and UV-vis absorption ratio at 415 nm (Soret peak) versus at 280 nm. The cutoff for pure proteins was  $A_{415}/A_{280} \geq 4$ . The protein was treated with 10-fold excess EDTA overnight at 4 °C to prepare the apo protein. Excess EDTA was removed by using the 10DG column (BioRad) and a buffer solution containing 20 mM Tris/HCl (pH 7.0) and 150 mM NaCl. For the preparation of fully Zn-metallated protein sample, ~2.5 equiv of ZnCl<sub>2</sub> (100 mM stock solution in ddH<sub>2</sub>O) was added to the protein, kept for ~1–3 h at 4 °C. The unbound Zn ions were removed by using a 10DG column and a buffer solution containing 20 mM Tris/HCl (pH 7.0) and 150 mM NaCl. Both apo and Zn bound protein samples were kept frozen at –80 °C after concentrating to a concentration of ~1 mM.

**Construction of Kanamycin-Resistant Vector for *cyt cb<sub>562</sub>* Protein Expression.** The original vector for *cyt cb<sub>562</sub>* expression is pET20b(+) (4034 bp) (22) and contains an ampicillin-resistance marker. To utilize ampicillin as a hydrolyzable substrate for *in vivo* screening, the vector was reconstructed with kanamycin-resistance sequence. The sequence for kanamycin-resistance was lifted from the pET24 vector (5236 bp, NEB). Both pET20b(+) and pET24 vectors were doubly digested with DraIII and AlwNI for 1 hr at 37 °C, using protocols recommended by the supplier (New England Biolabs, NEB). The digested product of pET 20b(+) was purified with 1.5% agarose gel electrophoresis

at 100 V for 1 hr and extracted using a DNA extraction kit (Promega), yielding 2414 and 1620 bp fragments. The pET24 kanamycin-resistant sequence (1487 bp) was also obtained using an identical procedure and was ligated to the piece from pET20b(+) (2414 bp) that contains the sequence for cyt *cb*<sub>562</sub> using T4 ligase (NEB). The ligated product was transformed to XL1-Blue *E. coli* cells and plated on the LB/agar plate containing 50 µg/mL of kanamycin. After overnight incubation at 37 °C, a few grown colonies were inoculated individually into ~30 mL of LB medium containing 50 µg/mL of kanamycin. The plasmid was extracted using the Miniprep kit from Qiagen and the DNA sequence was confirmed (Retrogen).

**Determination of Metal-Binding Properties of AB3 variants by ICP-OES and competition titrations.** Apo protein (~1 mM) was added 0 to 5-fold molar excess of ZnCl<sub>2</sub> (100 mM stock solution) and incubated for ~3 hrs at 22 °C. The solution was applied to a 10DG column using an elution solution containing 20 mM Tris/HCl (pH 7.0) and 150 mM NaCl to remove unbound metal ions. HNO<sub>3</sub> was added to the sample (~25-30 µM final concentration, 3 mL) to make a ~3% solution. A standard calibration curve for ICP-OES was prepared using 0-10 ppm Zn and Fe standard stock solutions (Ricca Chemical Company) prior to the analysis of protein solutions. The absorption of the each metal ion was monitored at >3 different wavelengths and in triplicate. The concentration of Fe, originating from the covalently bound heme cofactor, was used as an internal standard to determine monomeric protein concentration (Fig. S1A).

To determine the Zn affinities of the <sup>A104</sup>AB3 variant, a fluorescent metal chelate, MagFura-2, was used in competition assays. To a 1-mL solution of 20 mM MOPS (pH 7.0) and 150 mM NaCl, which was pre-treated with Chelex 100 (Biorad) for ~3 hrs prior to use, ~5 µM of metal-free MagFura-2 (Life Technologies,  $\epsilon_{366\text{ nm}} = 29\,900\text{ M}^{-1}\text{cm}^{-1}$ ) was added using pipette tips pre-washed with HNO<sub>3</sub>. To this solution, ~20-25 µM of <sup>A104</sup>AB3 apo protein was added from a concentrated stock solution, followed by aliquots of a ZnCl<sub>2</sub> stock solution (1 mM). The concentration of the ZnCl<sub>2</sub> stock solution was independently determined by titration with metal-free, 4-(2-pyridylazo)resorcinol PAR (~1.44 mM) and monitoring the changes at absorption at 500 nm ( $\epsilon_{500\text{ nm}}$  for (PAR)<sub>2</sub>Zn = 59100 cm<sup>-1</sup>M<sup>-1</sup>) (24). Following incubation for ~3-4 min to reach equilibrium, the change in the absorbance at 321 nm was used to measure the concentration of Zn-bound MagFura-2, which is in the equilibrium with <sup>A104</sup>AB3 protein (Fig. S6). The titration curves were fit to a consecutive two site binding model for protein, using Dynafit (37) as described previously (24). The experiments were performed in duplicate. The Zn binding constants for the <sup>A104/G57</sup>AB3 and <sup>A104/T105</sup>AB3 variants were determined using the same procedure (Table S5 and Fig. S11).

**Determination of the Oligomerization States of the Variants by Analytical Ultracentrifugation.** The samples for AUC analysis of Zn-protein complexes contained ~5 µM protein in a buffer solution consisting of 20 mM Tris/HCl (pH 7.0) and 150 mM NaCl. The measurements were made on a Beckman XL-A instrument using an An-60 Ti rotor. For each sample, 250-400 scans were obtained at 25 °C at 41 000 rpm. All data were processed using Heteroanalysis (University of Connecticut, Analytical Ultracentrifugation Facility) and SEDFIT software (38) with the following fixed parameters: buffer density ( $r$ ) = 1.0049 g/mL; buffer viscosity = 0.010214 poise;  $V_{\text{bar}}$  = 0.73084 (Fig S1B). The AUC experiments were also carried out with <sup>A104</sup>AB3 variant at

different pH's (pH 7, 9, and 10), relevant for enzymatic activity assays (Fig S10A) to demonstrate that the tetrameric species is still intact. The maximal sedimentation coefficients for the major species were 4.26, 4.59, 4.15 for pH 7, 9, and 10 conditions, respectively, accounting for 79%, 76%, and 70% abundance. The maximal sedimentation coefficients for the tetrameric species for <sup>A104/G57</sup>AB3 and <sup>A104/T105</sup>AB3 are 4.5 and 4.2, accounting for 90% and 76% abundance, respectively (Figs. S10B and S10C).

**X-ray Structure Determination.** Crystals of the Zn<sub>8</sub>:AB3<sub>4</sub> and Zn<sub>8</sub>:<sup>A104/G57</sup>AB3 complexes were obtained by sitting-drop vapor diffusion at 22 °C, using protein stock solutions (2 mM) pre-incubated with 2 equiv of ZnCl<sub>2</sub>. The following precipitant solutions were used: 18% PEG 400 in 100 mM Tris (pH 8.5) and 0.2 M MgCl<sub>2</sub> for AB3 and 27% (+/-)-2-methyl-2,4-pentanediol 400 in 100 mM Bis-Tris (pH 6.5) with 0.2 M CaCl<sub>2</sub> and 10 mM ampicillin for <sup>A104/G57</sup>AB3. The sitting drop contained 1 μL each of the protein stock solutions and precipitant solutions, and the well contained 300 μL of the precipitant solution. The crystals were frozen in liq. N<sub>2</sub> and diffraction data were collected at SSRL Beamlines 9-2 or 14-1 using 0.98 Å radiation at 100 K (see Table S3 for data collection and refinement statistics). Diffraction data were processed using iMosflm and Scala (39). Molecular replacement was carried out using Phaser (40) whereby the structure of the <sup>C96</sup>RIDC1 monomer (PDB 3IQ6) (24) was used as a search model. Rigid-body and restrained refinement with REFMAC5 (41) along with manual model rebuilding and metal/water/ligand placement with COOT produced the final models. For the Zn<sub>8</sub>:AB3<sub>4</sub> structure, 4-fold noncrystallographic symmetry (NCS) restraints were applied throughout the refinement process. The Ramachandran plots were calculated with PROCHECK (42). All figures (Figs 1, 3, S2, and S15) were produced with PYMOL (www.pymol.org).

**In Vitro Activity Assays for pNPA, ampicillin, and nitrocefin hydrolysis.** Activity assays for *p*-nitrophenyl acetate (pNPA) hydrolysis were carried out at 25 °C using an Agilent 8453 UV-vis spectrophotometer. The reaction of ~7 μM of protein with *p*-nitrophenyl acetate (pNPA, 0-1.5 mM, dissolved in CH<sub>3</sub>CN) at various pH's (pH = 7.0-10.0; 0.1M NaPi and borate buffers for pH 7.0-8.0 and pH 8.25-10.0 ranges, respectively) was monitored at 400-405 nm, where the hydrolyzed product, *p*-nitrophenolate strongly absorbs (Fig. S3A). Time-dependent optical changes were fit to a linear function to obtain initial rates, which were converted to initial molar rates. These rates were determined at various pNPA concentrations (Fig S3A). The data were fit to the Michaelis-Menten equation,  $v = k_{cat}[E]_0[S]/(K_M+[S])$ , where  $v$ ,  $[E]_0$ , and  $[S]$  are the rates, enzyme concentrations, and substrate concentrations, respectively, to determine  $k_{cat}$  and  $k_{cat}/K_M$  values (Fig. S3B). Given that some amino acids, such as serine or histidine, display basal pNPA hydrolysis activity, the net reactivity arising from the catalytic Zn sites was obtained by subtracting the initial product formation rate of the Zn-bound protein from that of the apo-protein under the identical conditions (pH, buffer component, temperature, and substrate concentrations). The rates for either apo or Zn-bound samples were measured in triplicate.

To determine the  $pK_a$  of Zn-H<sub>2</sub>O/OH<sup>-</sup> centers of <sup>A104</sup>AB3 variant, the pNPA hydrolysis assays were performed at various pH's (pH 7-10), using either 0.1 M sodium phosphate or sodium borate buffer at pH 7.0-7.5 or pH 8.0-10.0, respectively. The absorption coefficient at 405 nm for the deprotonated product, *p*-nitrophenolate varies depending on

pH conditions as  $12.8 \times 10^3 \text{ cm}^{-1} \text{ M}^{-1}$  at pH 7.5,  $16.2 \times 10^3 \text{ cm}^{-1} \text{ M}^{-1}$  at pH 8,  $17.8 \times 10^3 \text{ cm}^{-1} \text{ M}^{-1}$  at pH 9, and  $18.2 \times 10^3 \text{ cm}^{-1} \text{ M}^{-1}$  at pH >9.5 (43). The plot of hydrolysis rates vs. pH was fit to the following equation,  $y = (k_{\text{max}} * 10^{(\text{pH}-\text{pK}_a)}) / (1 + 10^{(\text{pH}-\text{pK}_a)})$ , where  $k_{\text{max}}$  indicates the maximum rate constant for the fully deprotonated (i.e.,  $\text{OH}^-$ ) species (Fig S3B). The data at pH 10 were excluded for the fit to estimate the single  $\text{pK}_a$  value for Zn- $\text{H}_2\text{O}/\text{OH}^-$  centers. To confirm that the enzymatic activity originated from the protein-bound Zn sites, the hydrolytic activities of free Zn ions were also measured by mixing various concentrations of free Zn ions with 750  $\mu\text{M}$  of pNPA at pH 9 (Fig. S3C). No dependence of the rate of pNPA hydrolysis on the Zn concentration was observed, indicating that the free Zn ion is not competent in catalysis. The hydrolytic activities of  $^{\text{A104/G57}}$ AB3 and  $^{\text{A104/T105}}$ AB3 for pNPA were also measured using the same procedure (Fig. S12).

To measure activities for ampicillin hydrolysis, the mixture of Zn-bound protein ( $\sim 7 \mu\text{M}$  in 0.1 M borate buffer) with freshly prepared ampicillin (dissolved in ddH<sub>2</sub>O) was injected to the C18 analytic column (Agilent Eclipse Plus C18, 3.5  $\mu\text{m}$ , 4.6 X 100 mm), using an Agilent Technologies 1260 Infinity HPLC workstation using the following elution profile: 90% H<sub>2</sub>O/10% CH<sub>3</sub>CN for 3 mins, followed by a linear gradient of 90% H<sub>2</sub>O/10% CH<sub>3</sub>CN to 10% H<sub>2</sub>O/90% CH<sub>3</sub>CN over 15 mins with 1 mL/min flow rate (Fig 2B). Injection were made every  $\sim 20$  mins to 1 hr for  $\sim 5$ -18 hrs at 25 °C and the quantitative analysis was done by using 220 nm detection and integrating the peak areas. The retention times of ampicillin and the hydrolyzed product were  $\sim 7.1$  and 7.8 mins, respectively, which were confirmed by ESI-MS and <sup>1</sup>H NMR (Fig S4). In ESI-MS for ampicillin (Fig S4A), M represents the molecular weight of ampicillin (349.1 g/mol). m/z: 129.1 (M+Cl<sup>-</sup>+4H<sup>+</sup>), 141.4 (M+2Cl<sup>-</sup>+5H<sup>+</sup>), 350.1 (M+H<sup>+</sup>), 372.1 (M+Na<sup>+</sup>). The mass for the hydrolyzed product, ampicilloic acid, was represented as (M+H<sub>2</sub>O): 114.8 ((M+H<sub>2</sub>O)+4Na<sup>+</sup>), 145.3 ((M+H<sub>2</sub>O)+3Na<sup>+</sup>), 206.5 ((M+H<sub>2</sub>O)+2Na<sup>+</sup>), 237.6 ((M+H<sub>2</sub>O)+2Na<sup>+</sup>+3H<sup>+</sup>+BO<sub>3</sub><sup>3-</sup>). <sup>1</sup>H NMR spectroscopy was performed on Varian 400 MHz instrument and the spectra were calibrated to a residual solvent. <sup>1</sup>H NMR for ampicillin (Fig S4B):  $\delta$  9.38-9.29 (d, 1H), 7.64-7.25 (m, 5H), 5.58-5.49 (dd, 1H), 5.43-5.36 (d, 1H), 5.04 (s, 1H), 4.16 (s, 1H), 1.55-1.28 (d, 6H). The solvent peaks, H<sub>2</sub>O and DMSO, at 3.34 and 2.49 ppm, respectively, were marked with asterisks. <sup>1</sup>H NMR for ampicilloic acid:  $\delta$  8.64-8.59 (d, 1H), 7.86-7.81 (d, 1H), 7.39-7.27 (m, 5H), 5.10-5.06 (d, 1H), 4.93 (s, 1H), 3.85-3.81 (t, 1H), 3.59 (s, 1H), 1.54 (s, 3H), 1.20 (s, 3H).

A linear fit to the time-dependent changes in the concentration of the substrate was used to obtain the initial rate of substrate consumption. The specific ampicillin hydrolysis activity was obtained from the reaction with 750  $\mu\text{M}$  of ampicillin at pH 9.0, whereby the initial rates were converted to specific activities by dividing by the mass of protein used for the reaction, 0.0084 mg (Fig S9). To estimate the uncatalyzed rate of ampicillin hydrolysis, the rate of ampicillin consumption was measured over  $\sim 5$ -18 hrs with various substrate concentrations under identical conditions (buffer composition and temperature) as the enzymatic assay, except that the protein was not included. A linear fit was applied to obtain a slope, which represents the uncatalyzed rate constant.

The hydrolytic rates of the Zn-complexed proteins were determined at various ampicillin concentrations (Fig 2C, 2F, and S14). The data were fit to the Michaelis-Menten equation,  $v = k_{\text{cat}}[\text{E}]_0[\text{S}] / (K_M + [\text{S}])$ , where  $v$ ,  $[\text{E}]_0$ , and  $[\text{S}]$  are the rates, enzyme

concentrations, and substrate concentrations, respectively, to determine  $k_{\text{cat}}$  and  $k_{\text{cat}}/K_M$  values (Fig. 2F and Table 1).

To determine the  $pK_a$  of Zn-H<sub>2</sub>O/OH<sup>-</sup> centers of <sup>A104/G57</sup>AB3 and <sup>A104/T105</sup>AB3 variants, the ampicillin hydrolysis assays were performed at various pH's (pH 7-10), using either 0.1 M sodium phosphate or sodium borate buffer at pH 7.0-7.5 or pH 8.0-10.0, respectively. The reaction was initiated by mixing either <sup>A104/G57</sup>AB3 or <sup>A104/T105</sup>AB3 protein (7 μM) with 750 μM of ampicillin. To obtain the net activities of the proteins, first, the background rate of ampicillin hydrolysis was measured using the <sup>C96</sup>RIDC1 variant, which lacks the catalytic Zn sites. Then, this baseline rate was subtracted from the observed rates obtained with Zn-protein complexes. The plot of hydrolysis rates vs pH was fit to the following equation,  $y = (k_{\text{max}} * 10^{(\text{pH}-\text{p}K_a)}) / (1 + 10^{(\text{pH}-\text{p}K_a)})$ , where  $k_{\text{max}}$  indicates the maximum rate constant for the fully deprotonated (i.e., OH<sup>-</sup>) species (Fig S13).

Hydrolytic activity with nitrocefin was measured by monitoring the formation of the hydrolyzed product at 490 nm at 25 °C, upon the mixing of the Zn-complex of <sup>A104/G57</sup>AB3 (7 μM) with nitrocefin (dissolved in H<sub>2</sub>O:DMSO=1:2) in a 0.1 M sodium borate buffer solution (pH 9) (Fig S17). The  $\epsilon_{490}$  values for substrate and product, 1520 cm<sup>-1</sup>M<sup>-1</sup> and 17200 cm<sup>-1</sup>M<sup>-1</sup>, respectively (44), were used to calculate the hydrolytic rate constants. The reaction with apo-<sup>A104/G57</sup>AB3 was also carried out under identical conditions to obtain the net hydrolytic activity of Zn-OH site.

#### **Characterization of Proteins from Periplasmic Extraction and Purification.**

Periplasmic extraction of the <sup>A104</sup>AB3 variant was carried out as previously described (45). Briefly, *E. coli* cells expressing the <sup>A104</sup>AB3 protein were sedimented by centrifugation at 5000 rpm, 4 °C. The cell paste was washed three times with ice-cold buffer solution containing 10 mM Tris/HCl (pH 7.3) and 30 mM NaCl. The cell pellet was then resuspended with 10 volumes (v/w) of a 33 mM Tris/HCl (pH 7.3) buffer solution, and subsequently added an equal volume of the the same buffer solution now supplemented with 40% sucrose and 0.4 mM EDTA. The suspension was gently shaken for 10 mins at room temperature and centrifuged at 4 °C. To remove residual EDTA, the pellet was washed with the 33 mM Tris/HCl (pH 7.3) buffer solution. The pellet was then resuspended with 20 volumes of ice-cold buffer containing 0.5 mM MgCl<sub>2</sub>, and gently swirled for 10 mins to effect the lysis of the outer membrane, followed by centrifugation at 4 °C for 20 min. Iodoacetamide was added in excess in the last step of periplasmic extraction so that any free thiol-containing proteins, such as the monomeric <sup>A104</sup>AB3 variants could be trapped to prevent post-lytic oligomerization. To confirm that no free thiol-species remains in the solution, Ellman's reagent (5,5'-dithiobis-(2-nitrobenzoic acid)) was added. No spectral changes were observed, which indicated that the reaction with iodoacetamide was complete. The protein contained in the extract was immediately isolated using a Q sepharose column, and applied to a Superdex75 size exclusion chromatography column for the determination of the oligomerization state. To determine the retention time for monomeric, dimeric, and tetrameric species, MBPC1, <sup>A104/T96</sup>AB3, and Zn<sub>8</sub>.<sup>A104</sup>AB3<sub>4</sub> variants, respectively, were also run as standards (Fig S5A). The oligomeric state of MBPC1 in the absence of Zn has been previously characterized with analytical ultracentrifugation to be a monomer (1.8 S) (46). <sup>A104/T96</sup>AB3 protein was

prepared by site-directed mutagenesis as an indicator for the dimeric state, which was independently confirmed by analytical ultracentrifugation (2.3 S).

To prepare fully metallated <sup>A104</sup>AB3 oligomers and to measure their Zn occupancy, the BL21(DE3) *E. coli* cells with the *ccm* cassette were grown in LB media supplemented with 50 μM of ZnCl<sub>2</sub>. The proteins extracted from the periplasm were purified using a modified procedure from what is described above, which avoids using any anionic exchange columns for pre-purification, because the Q Sepharose resin was found to extract Zn ions from proteins. The periplasmic extract was directly applied to a size exclusion column (AcA 50), which yielded protein AB3 oligomers with >60% purity, based on the SDS-PAGE gel and UV-vis spectrum of the sample. Any impurities eluted with the targeted <sup>A104</sup>AB3 variant did not contain any metal ions, indicating that all detected metal ions (by ICP-OES) originated from the AB3 oligomers. The Fe concentration was used as an internal indicator for AB3 monomer concentration as each monomer contains a single, covalently bound heme cofactor (Fig S5B).

**Construction of Saturated Mutant Libraries of <sup>A104</sup>AB3.** To generate random point-mutant libraries at individual active site positions for <sup>A104</sup>AB3 protein, previously published saturated-mutagenesis protocols (29) were followed, whereby a kanamycin-resistant vector (*vide supra*) carrying the <sup>A104</sup>AB3 gene was used. The primers used for PCR to modify the residues 57, 60, 104, and 105 at <sup>A104</sup>AB3 were as follows, where N = A, C, G or T; K = G or T; M = A or C:

57: 5'-CG GAC AGC CCG **NNK** ATG CAC GAT TTC-3' and 5'-GAA ATC GTG CAT **MNN** CGG GCT GTC CG-3'

60: 5'-CCG GAA ATG CAC **NNK** TTC CGC CAC GG-3' and 5'-CC GTG GCG GAA **MNN** GTG CAT TTC CGG-3'

104: 5'-C AAC CAT TGC CAC CAG NN **KTA** TCG TTA ATT CCT C-3' and 5'-GA GGA TTA ACG ATA **MNN** CTG GTG GCA ATG GTT G-3'

105: 5'-CAT TGC CAC CAG GCG **NNK** CGT TAA TTC CTC ATT TC-3' and 5'-G AAAT GAG GAA TTA ACG **MNN** CGC CTG GTG GCA ATG-3'

Multiple rounds of PCR were performed at various annealing temperatures (57-59 °C). To minimize the chance of obtaining the same sequence as the parent template, the PCR products were digested with DpnI for 1 hr at 37 °C and transformed into XL1-Blue or DH5α competent cells. To cover 95% of complete single mutant library, greater than 100 colonies were picked from the LB/agar plates, yielding the mixture of plasmids that contained random codons for the targeted residue. The randomized codon of the plasmid mixtures was confirmed by DNA sequencing (Fig. S7).

***In Vivo* Screening of β-Lactamase Activities.** Randomized plasmid libraries were transformed into BL21(DE3) *E. coli* cells, which contained the *ccm* (cytochrome c maturation) cassette and plated on LB/agar plates containing 50 mg/L of kanamycin and 30 mg/L of chloramphenicol. Greater than 100 colonies were picked and inoculated into LB medium solutions containing kanamycin and chloramphenicol at the same concentrations as described above. 50 μM of ZnCl<sub>2</sub> was added into the culture media and the cells were grown at 37 °C for ~20 hrs. Upon reaching an OD<sub>600</sub> ~1.5, 40 μL aliquots of the cultures were inoculated on the LB/agar plates containing 50 mg/L of kanamycin,

30 mg/L of chlorophenicol, 50  $\mu\text{M}$   $\text{ZnCl}_2$ , 25  $\mu\text{M}$  IPTG, and various concentrations of ampicillin (0-1.6 mg/L) and the plates were incubated at 37 °C for ~30 hrs. Due to the leaky expression system, IPTG was not necessary to express the protein, but was added for *in vivo* experiments to ensure immediate protein expression during cell growth. The colonies grown on the plates were individually inoculated into ampicillin-free LB media for miniprep and sequencing. The sequencing results of the surviving cells are summarized in Figs. 3E and S8. To obtain more accurate statistics of the screening results, each codon, rather than amino acid, were counted so that there is no bias for the amino acids that are encoded by more than one codon. The dominant and minor outputs for each amino acid were shown with red and white bars in Fig. S8, respectively.

**Building a Docking Model for  $\text{A}^{104/\text{G}57}\text{AB3}$  Variant with Ampicillin.** The coordinates for ampicillin were generated using the PRODRG server (47). The ampicillin molecule was set to have the freedom of rotation at every carbon atom except for those comprising of  $\beta$ -lactam and arene ring. Autodock Vina (48) was utilized to predict potential binding sites for ampicillin to the protein surface. The size of grid box was set to 22 X 24 X 28  $\text{\AA}^3$ . Among the multiple possible conformations, three of them, exhibiting the carbonyl group of the  $\beta$ -lactam close to the Zn-OH, are shown as possible docking conformations (Fig. S15C).

**Determination of 1,8-ANS Interactions of the Zn-complexed Variants.** The emission spectra of 1-anilinonaphthalene-8-sulfonate (ANS) were recorded at 22 °C between 400 and 730 nm upon the excitation at 386 nm (49) using a Horiba FluoroLog Spectrophotometer. A stock solution of 1,8-ANS (77 mM in DMSO) was freshly prepared and its concentration was spectrophotometrically determined using  $\epsilon_{350\text{ nm}} = 5000\text{ M}^{-1}\text{cm}^{-1}$  (50). Either 1,8-ANS (14  $\mu\text{M}$ ) or the mixture of 1,8-ANS with protein samples as the ratio of 1:2 were prepared in 3 mL of a buffer solution containing 20 mM Tris/HCl (pH 7.0) and 150 mM NaCl. The protein-free, 1,8-ANS sample displayed a characteristic emission with  $\lambda_{\text{max}} = 520\text{ nm}$ , which immediately shifted to 470 nm with a large concomitant increase in intensity upon addition of  $\text{Zn}_8\text{.A}^{104/\text{G}57}\text{AB3}_4$  (Fig S16). The increase in the fluorescence with blue shift is indicative of the interaction of 1,8-ANS with accessible hydrophobic surface of the protein.

## Supplementary Figures

**Fig S1.** Characterization of the metal content and oligomerization properties of various cyt *cb*<sub>562</sub> constructs.

**Fig S2.** Various views of the Zn<sub>8</sub>:AB<sub>3</sub><sub>4</sub> crystal structure.

**Fig S3.** Hydrolysis of pNPA by Zn<sub>8</sub>:<sup>A104</sup>AB<sub>3</sub><sub>4</sub>.

**Fig S4.** ESI-MS and NMR spectra of ampicillin and its hydrolysis product.

**Fig S5.** Determination of the oligomeric state (A, size exclusion chromatography) and the metal content (B, ICP-OES) of the <sup>A104</sup>AB<sub>3</sub> assembly extracted from the *E. coli* periplasm.

**Fig S6.** A representative competitive Zn-binding isotherm of <sup>A104</sup>AB<sub>3</sub> and MagFura-2,

**Fig S7.** Representative sequencing results of saturated single variant library of <sup>A104</sup>AB<sub>3</sub>, showing the randomization of the codons for the selected residues.

**Fig S8.** Frequencies of ampicillin survival by cells expressing saturated <sup>A104</sup>AB<sub>3</sub> single mutant libraries.

**Fig S9.** *In vitro* β-lactamase activities of selected variants.

**Fig S10.** Characterization by sedimentation velocity of the oligomerization states of <sup>A104</sup>AB<sub>3</sub> variants in the presence of 2 equivalents of Zn.

**Fig S11.** Competitive Zn-binding isotherms for <sup>A104/G57</sup>AB<sub>3</sub> and <sup>A104/T105</sup>AB<sub>3</sub>.

**Fig S12.** Hydrolysis of pNPA by Zn<sub>8</sub>:<sup>A104/G57</sup>AB<sub>3</sub><sub>4</sub> and Zn<sub>8</sub>:<sup>A104/T105</sup>AB<sub>3</sub><sub>4</sub>.

**Fig S13.** pH-dependent ampicillin hydrolysis rates of AB<sub>3</sub> variants and control species.

**Fig S14.** Hydrolysis of ampicillin by other single variants of Zn<sub>8</sub>:<sup>A104</sup>AB<sub>3</sub><sub>4</sub>.

**Fig S15.** X-ray crystal structure of Zn<sub>8</sub>:<sup>A104/G57</sup>AB<sub>3</sub><sub>4</sub> and the docking models of ampicillin binding near the peripheral Zn sites.

**Fig S16.** Fluorescence emission spectra of 1-anilinonaphthalene-8-sulfonate (ANS) in the absence and presence of Zn-bound assemblies, Zn<sub>4</sub>:<sup>C96</sup>RIDC1<sub>4</sub>, Zn<sub>8</sub>:AB<sub>3</sub><sub>4</sub>, and Zn<sub>8</sub>:<sup>A104/G57</sup>AB<sub>3</sub><sub>4</sub>.

**Fig S17.** Nitrocefin hydrolysis activity of Zn<sub>8</sub>:<sup>A104/G57</sup>AB<sub>3</sub><sub>4</sub>.

## Supplementary Tables

**Table S1.** Triads of potential Zn-binding residues on Zn<sub>4</sub>:<sup>96</sup>CRIDC1<sub>4</sub>. The triad variants prepared for this study are shown in bold with their abbreviated names in parentheses.

**Table S2.** DNA primers used for site-directed mutagenesis.

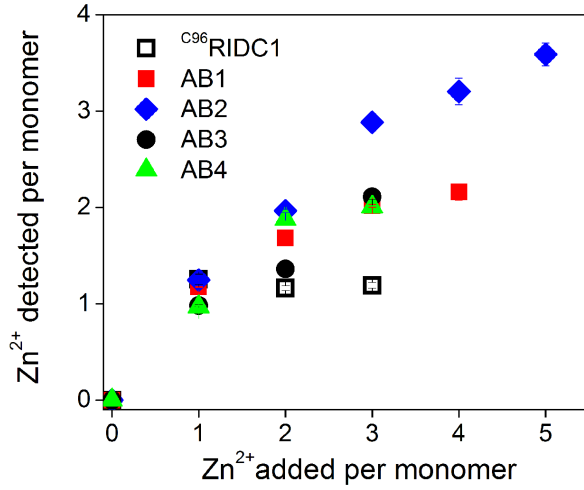
**Table S3.** Crystallographic data collection and refinement statistics.

**Table S4.** Previously published pNPA hydrolysis activities of various proteinaceous and non-proteinaceous catalysts for comparison.

**Table S5.** Dissociation constants for the Zn complexes of <sup>A104/G57</sup>AB3 and <sup>A104/T105</sup>AB3 variants.

**Fig. S1.** Characterization of the metal content and oligomerization properties of various *cyt cb<sub>562</sub>* constructs.

(A)



(B)

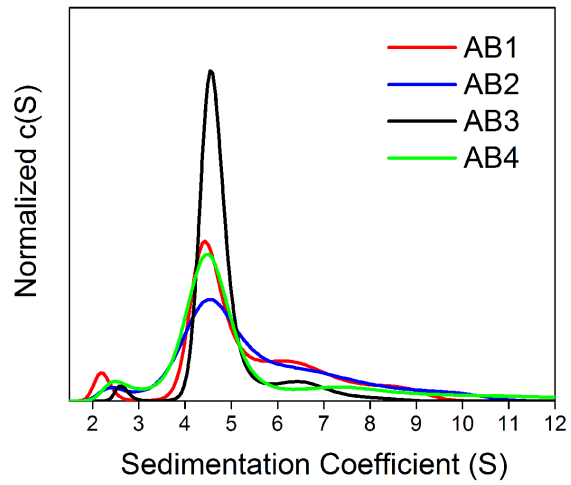
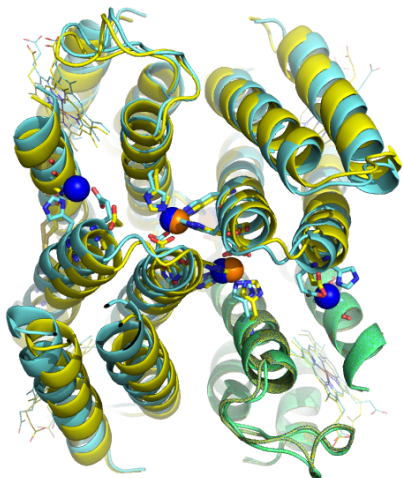


**Fig. S2.** Various views of the  $Zn_8:AB3_4$  structure.

(A) Superposition of  $Zn_8:AB3_4$  with  $Zn_4:^{96}C$ RIDC1<sub>4</sub> (PDB 3IQ6).  $Zn_8:AB3_4$  with  $Zn_4:^{96}C$ RIDC1<sub>4</sub> are colored in cyan and yellow, respectively. The Zn atoms in  $Zn_8:AB3_4$  with  $Zn_4:^{96}C$ RIDC1<sub>4</sub> are colored in blue and orange, respectively.



(B) Close-up view of the four peripheral Zn-coordination sites engineered for catalysis in ball-and-stick (left), the corresponding  $2F_o - F_c$  electron density map contoured at  $1\sigma$  (cyan, middle), and surface/space-filling representations (right). The Zn atom is shown as a navy sphere. The Zn coordinating residues (86, 89, 100) and the surrounding residues (57, 60, 104, 105) are shown as pink and yellow sticks, respectively. To illustrate the potential accessibility to the Zn site from bulk solvent, surface representation of the K104 side chain was omitted.

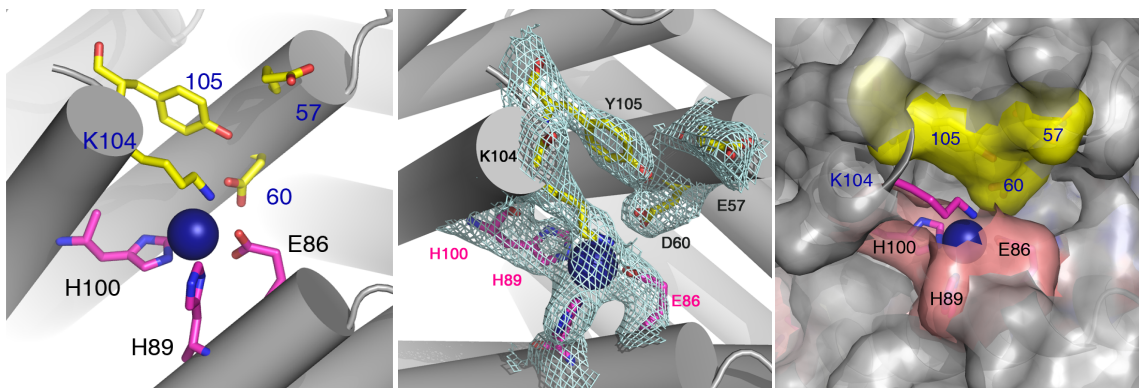
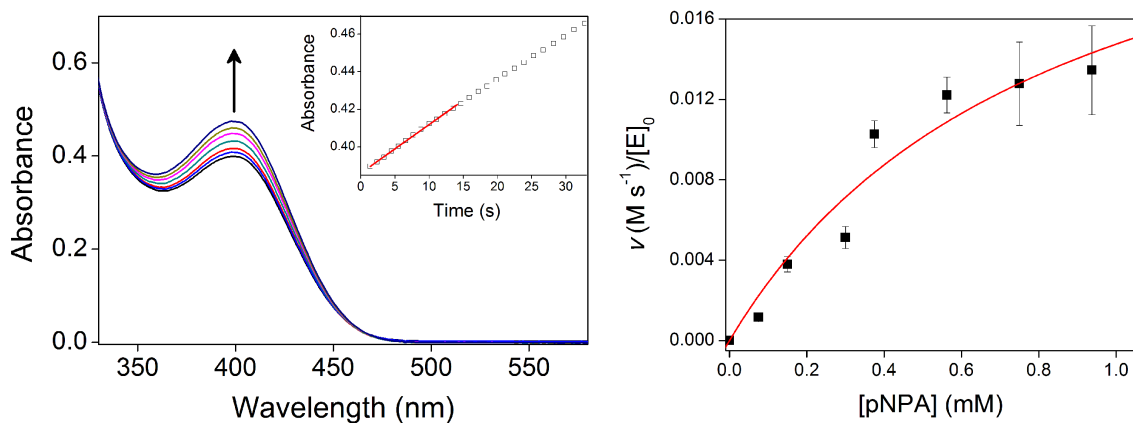
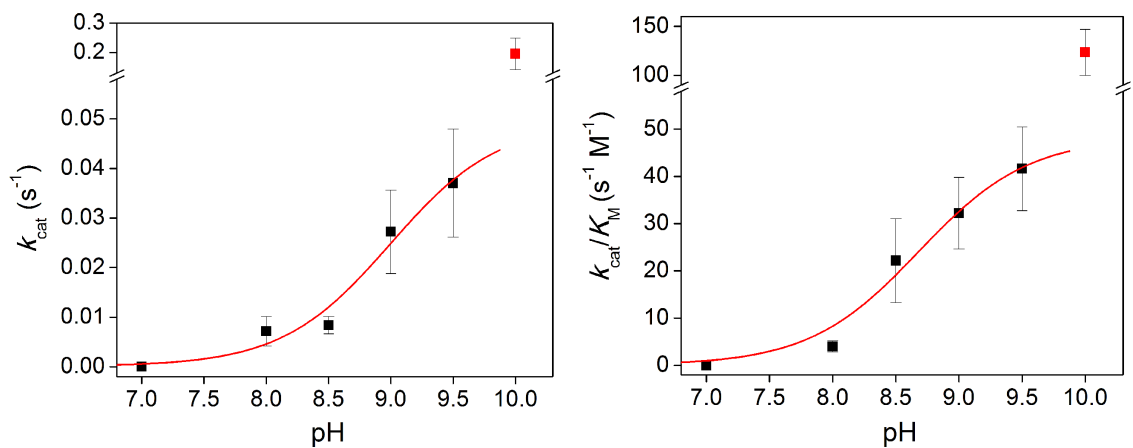


**Fig. S3.** Hydrolysis of pNPA by  $\text{Zn}_8^{\text{A}104}\text{AB}_3_4$ .

(A) Representative time-dependent UV-vis spectra during the reaction of  $\text{Zn}_8^{\text{A}104}\text{AB}_3_4$  with pNPA and a Michaelis-Menten plot for the reaction in 0.1 M sodium borate buffer (pH 9) at 25 °C.



(B) pH-dependent Michaelis-Menten kinetic parameters for the hydrolysis of pNPA by  $\text{Zn}_8^{\text{A}104}\text{AB}_3_4$ .



(C) The lack of pNPA hydrolytic activity by the free Zn ion.

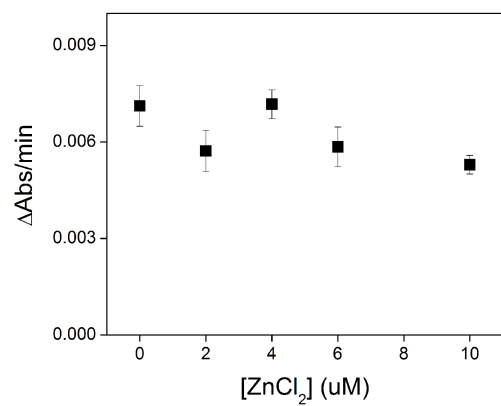
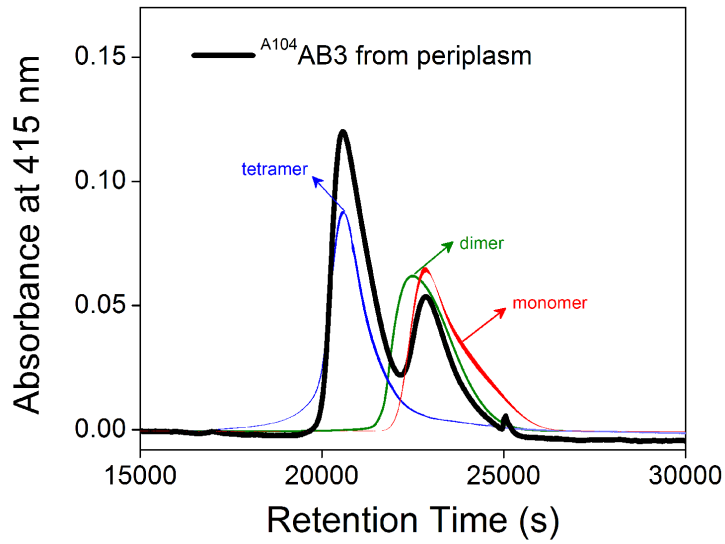




**Fig. S5.** Determination of the oligomeric state (A, size exclusion chromatography) and the metal content (B, ICP-OES) of the  $A^{104}$ AB3 assembly extracted from the *E. coli* periplasm.

A) Size-exclusion chromatography



B) Metal content

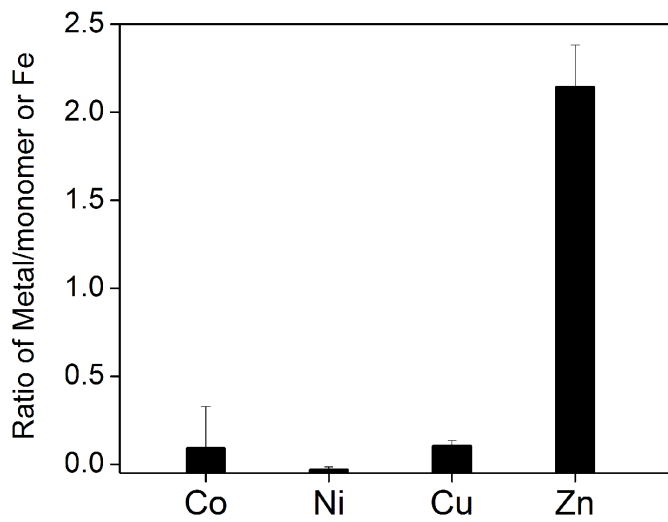


**Fig. S6.** A representative competitive Zn-binding isotherm of  $^{A104}$ AB3 and MagFura-2.

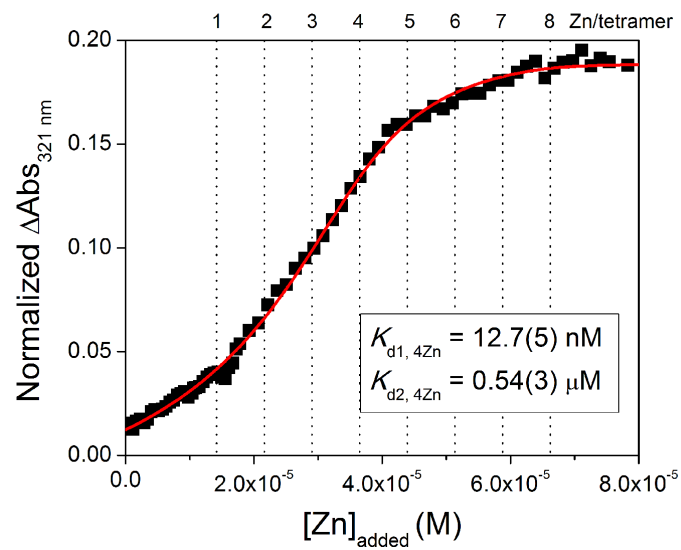
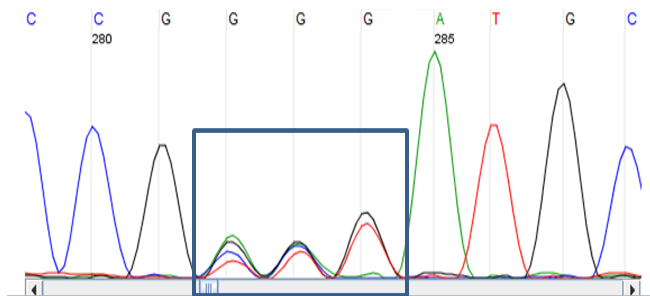
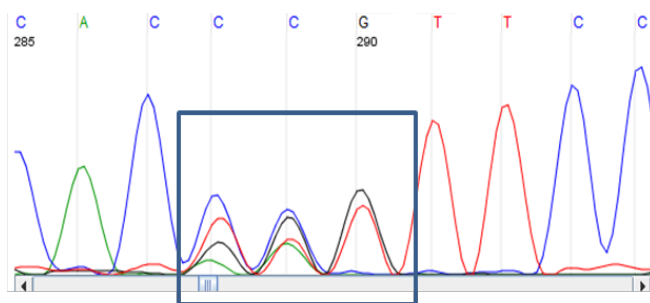


**Fig. S7.** Representative sequencing results of the saturated single variant library of  $\Delta^{104}$ AB3, showing the randomization of the codons for the selected residues (shown with a box).

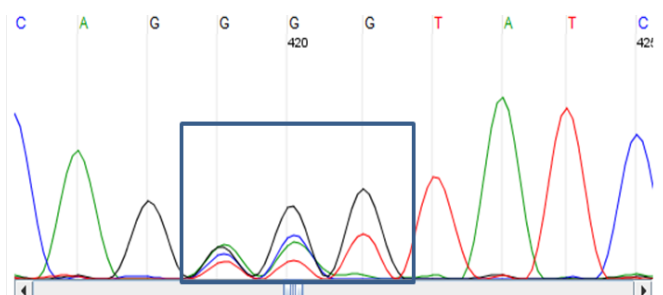
(A) 57 residue



(B) 60 residue



(C) 104 residue



(D) 105 residue

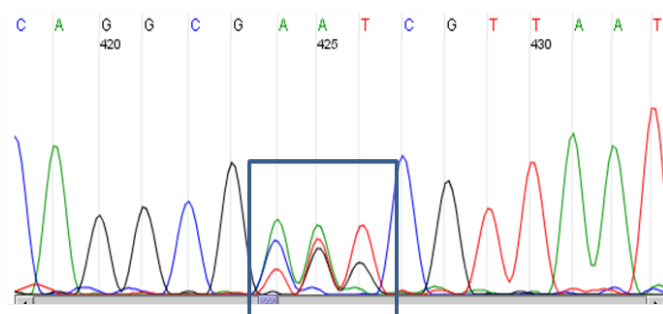


**Fig. S8.** Frequencies of ampicillin survival by cells expressing saturated  $A^{104}$ AB3 single mutant libraries. To obtain more accurate statistics of the screening results, each codon, rather than amino acid, were counted so that there is no bias for the amino acids that are encoded by more than one codon. The dominant and minor outputs for each amino acid were shown with red and white bars, respectively. Original residues are marked with asterisks.

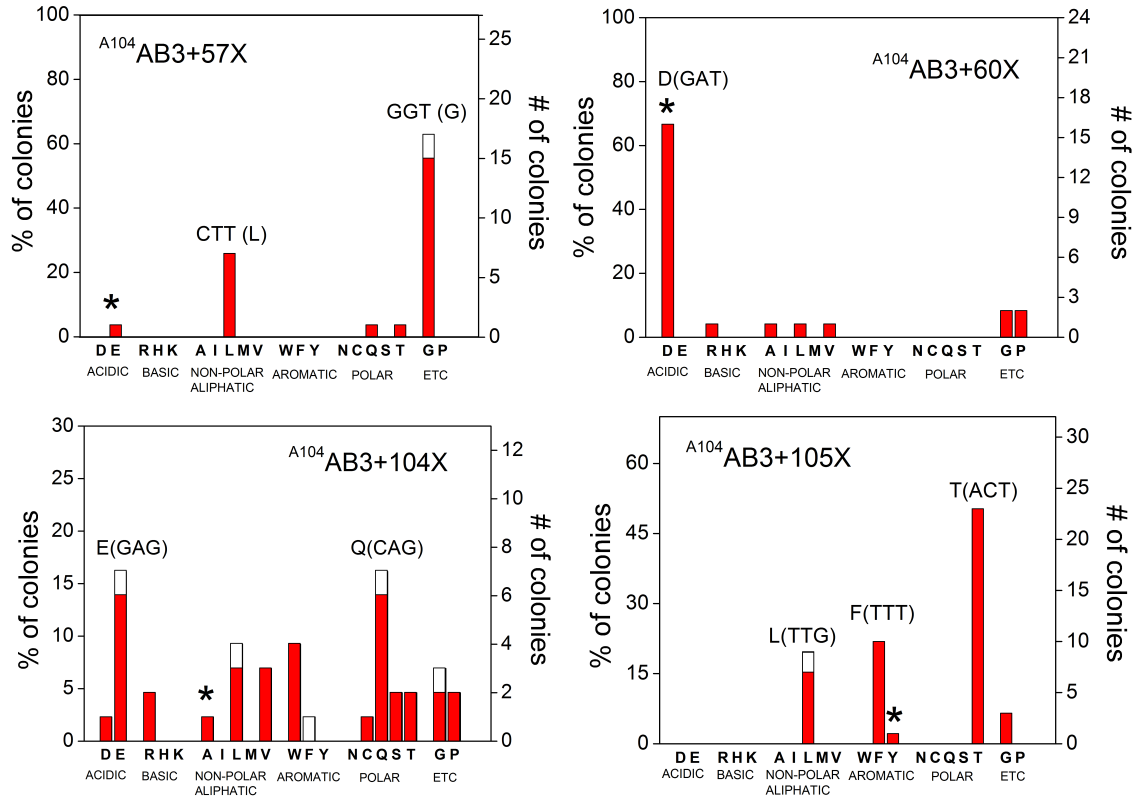


**Fig. S9.** *In vitro*  $\beta$ -lactamase activities of selected variants (in their Zn-complexed forms unless indicated).

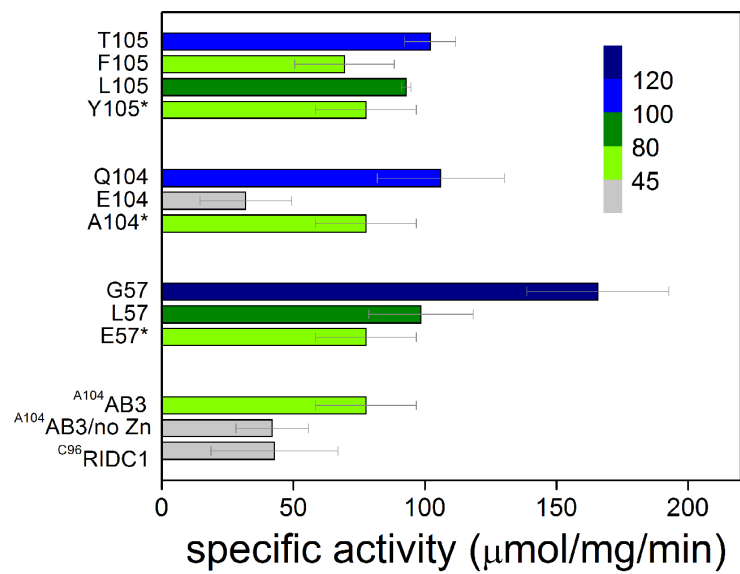
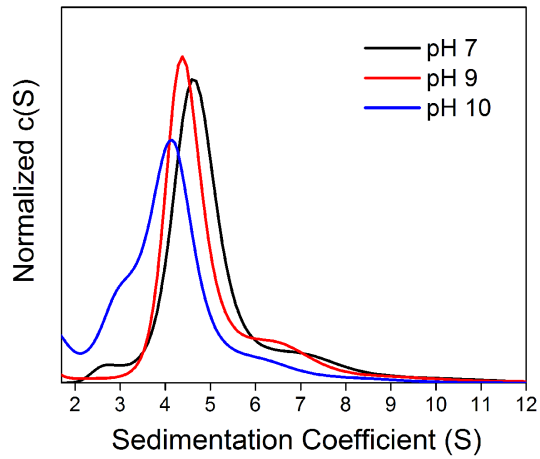


**Fig. S10.** Characterization by sedimentation velocity of the oligomerization states of  $A^{104}$ AB3 variants in the presence of 2 equivalents of Zn.

(A)  $A^{104}$ AB3 at pH 7, 9 and 10.



(B)  $A^{104/G57}$ AB3 (left) and  $A^{104/T105}$ AB3 (right)

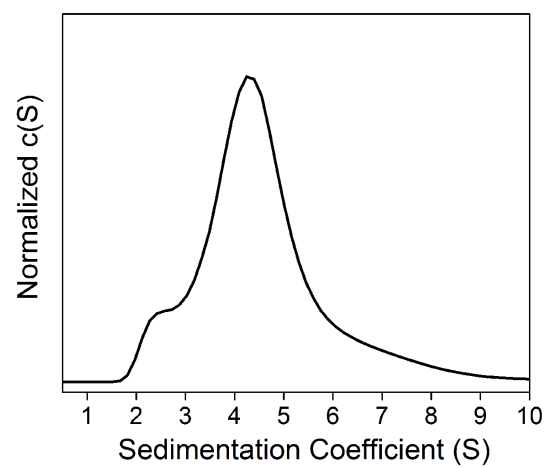
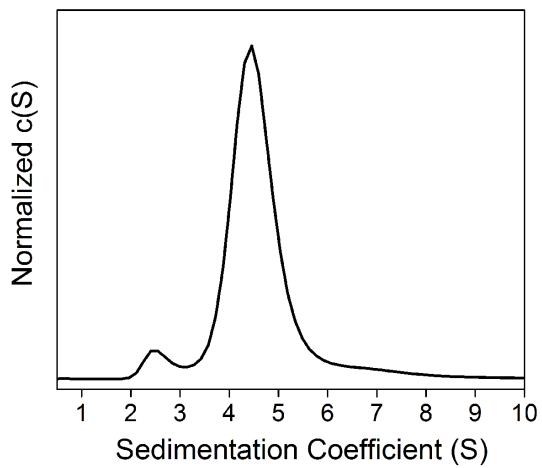
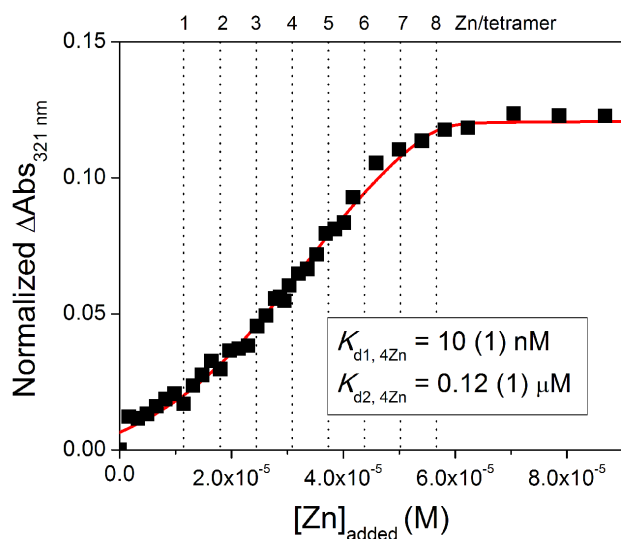


**Fig. S11.** Competitive Zn-binding isotherms for  $A^{104/G57}AB3$  and  $A^{104/T105}AB3$ .

(A)  $A^{104/G57}AB3$  (26  $\mu\text{M}$ ); MagFura-2 (5.31  $\mu\text{M}$ ).



(B)  $A^{104/T105}AB3$  (28  $\mu\text{M}$ ); MagFura-2 (5.72  $\mu\text{M}$ ).

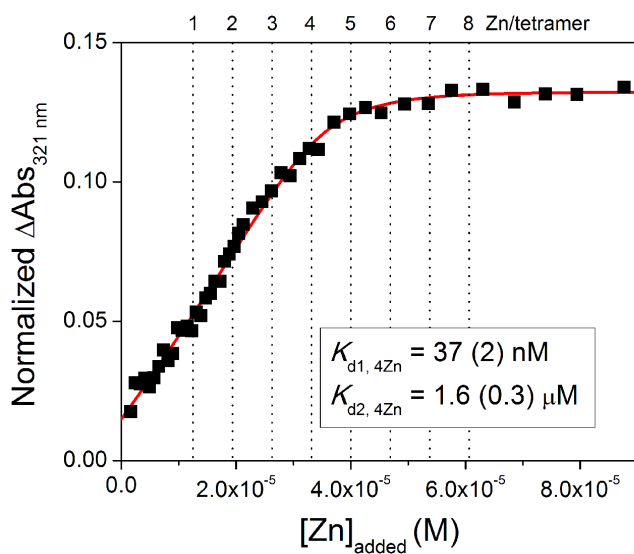
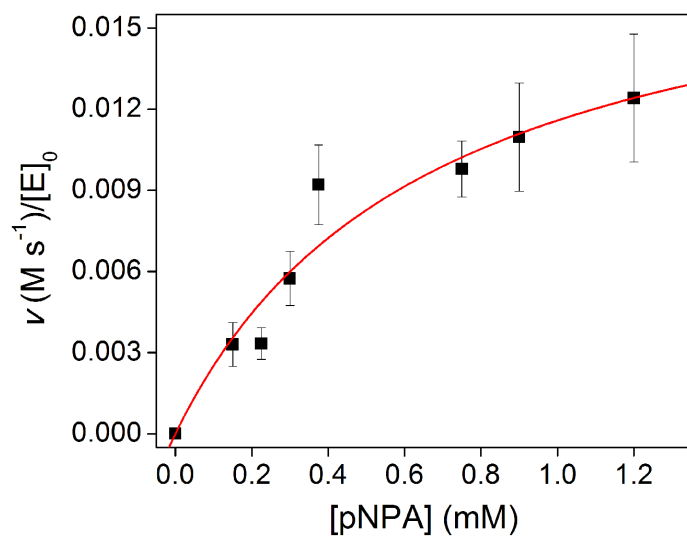


**Fig. S12.** Hydrolysis of pNPA by  $\text{Zn}_8^{\cdot\text{A}104/\text{G}57}\text{AB}_3_4$  and  $\text{Zn}_8^{\cdot\text{A}104/\text{T}105}\text{AB}_3_4$ .

(A)  $\text{Zn}_8^{\cdot\text{A}104/\text{G}57}\text{AB}_3_4$



(B)  $\text{Zn}_8^{\cdot\text{A}104/\text{T}105}\text{AB}_3_4$

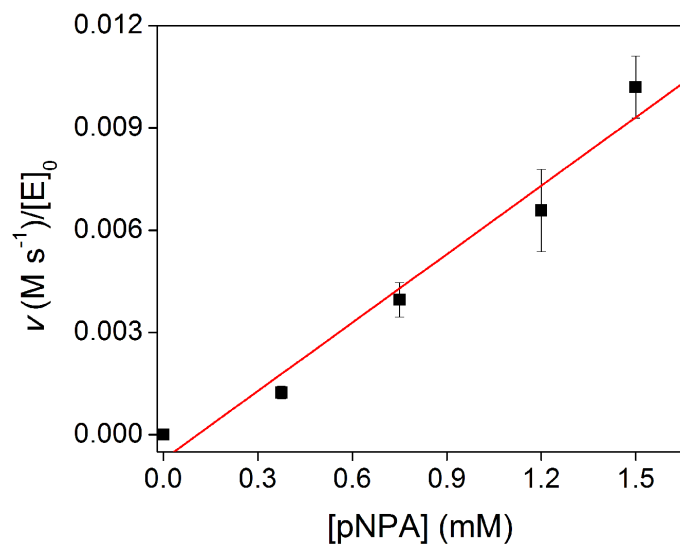


**Fig. S13.** pH-dependent ampicillin hydrolysis rates of the Zn complexes of AB3 variants and control species.

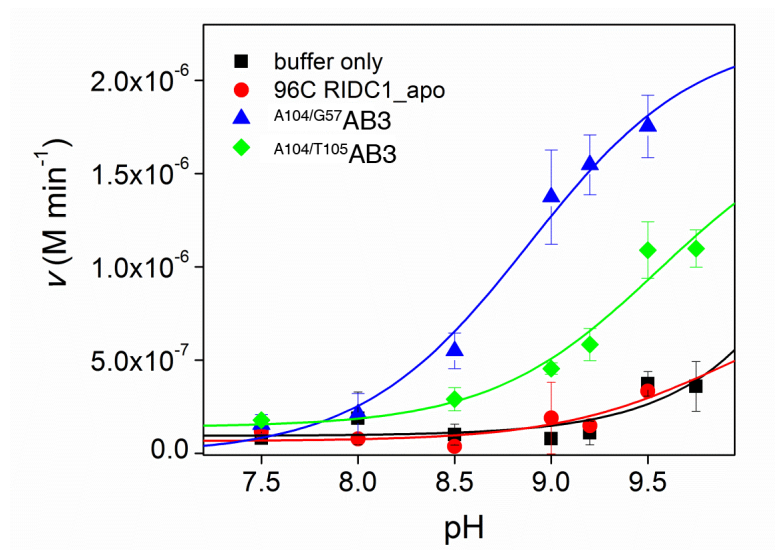
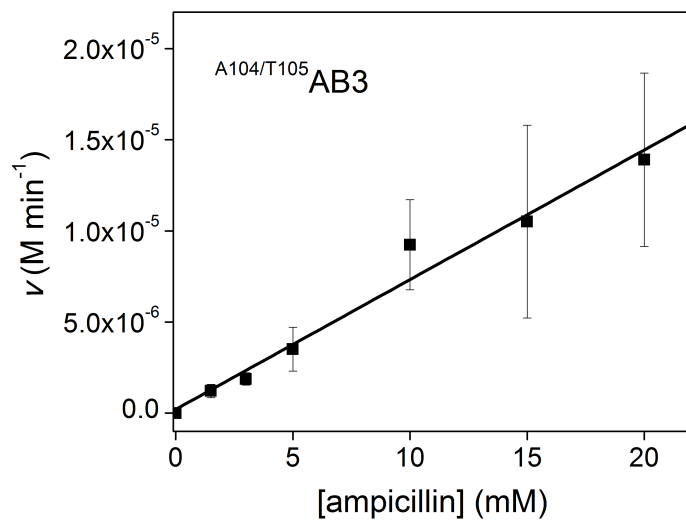
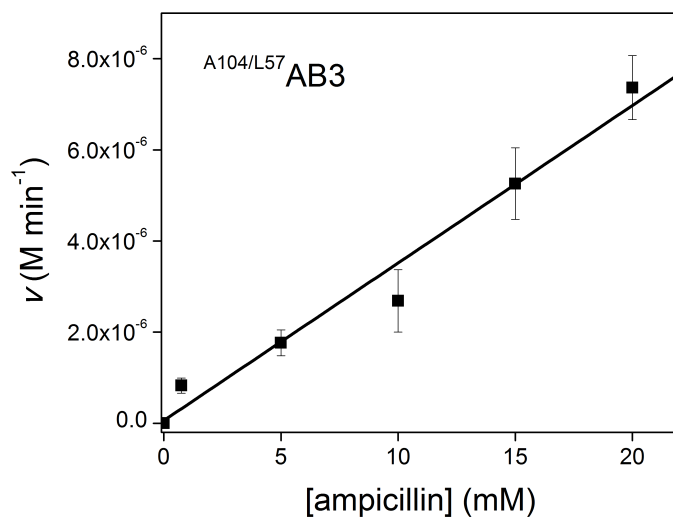


**Fig. S14.** Hydrolysis of ampicillin by single variants of  $\text{Zn}_8^{\text{A104}}\text{AB}_3$  (other than  $\text{Zn}_8^{\text{A104/G57}}\text{AB}_3$ ). The data were fit to either a linear (black) or Michaelis-Menten equation (red).

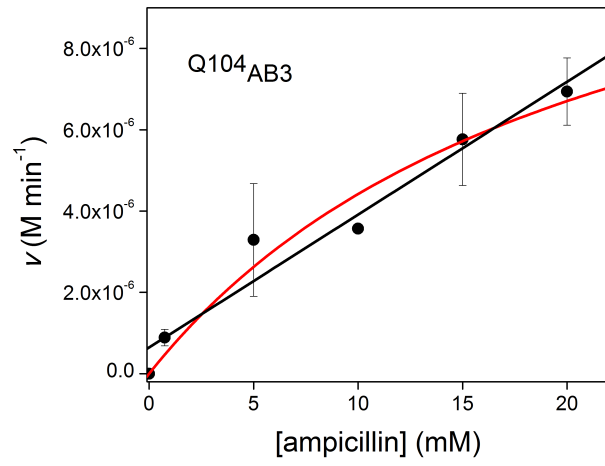
(A)  $\text{Zn}_8^{\text{A104/T105}}\text{AB}_3$



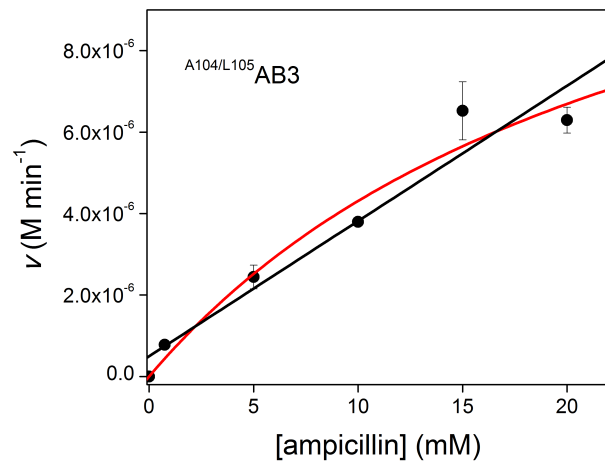
(B)  $\text{Zn}_8^{\text{A104/L57}}\text{AB}_3$



(C)  $\text{Zn}_8^{\text{Q104}}\text{AB3}_4$



(D)  $\text{Zn}_8^{\text{A104/L105}}\text{AB3}_4$



(E)  $\text{Zn}_8^{\text{A104/F105}}\text{AB3}_4$

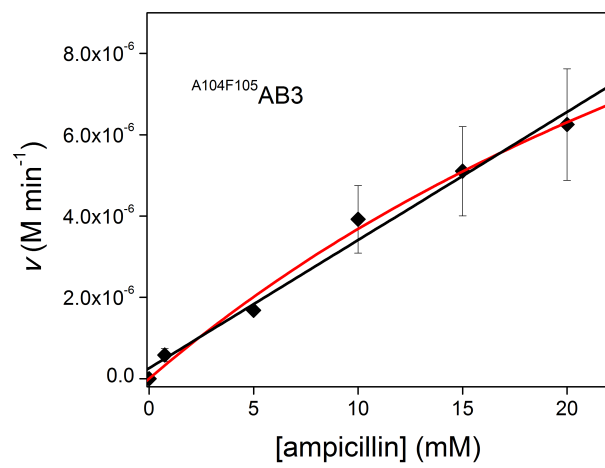
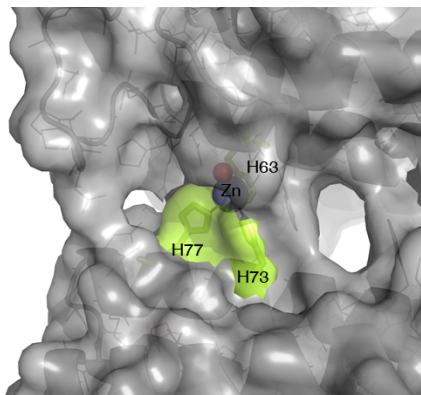
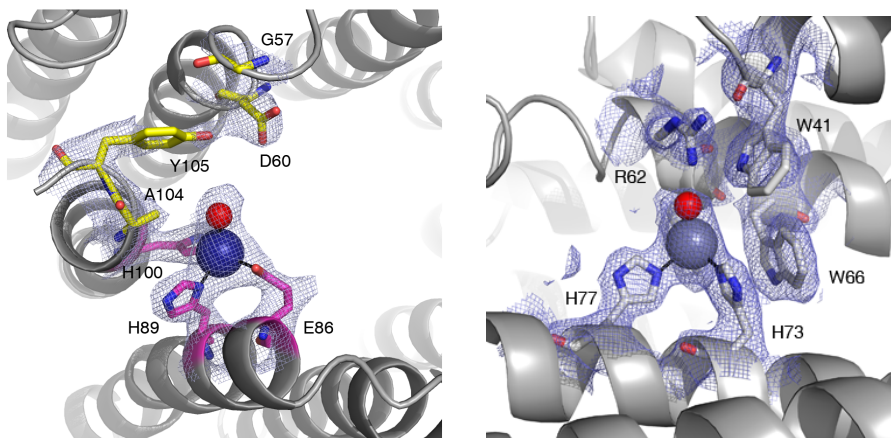


**Fig. S15.** X-ray crystal structure of  $\text{Zn}_8^{\cdot\text{A104/G57}}\text{AB3}_4$  and the docking models of ampicillin binding near the peripheral Zn sites.

(A) Close-up view of the structural Zn-coordination sites shown as surface representation. The Zn-coordinating residues (H63, H73, H77) are shown as green sticks. The Zn center and the coordinated solvent molecule are shown as navy and red spheres, respectively.



(B) Close-up view of the four catalytic Zn-coordination sites (left) and the four structural Zn-coordination sites (right), and the corresponding  $2F_o - F_c$  electron density maps contoured at  $1\sigma$  (cyan). The Zn atom and the Zn-bound solvent molecule at the catalytic sites are shown as navy and red spheres, respectively. The residues at the catalytic sites are shown with yellow sticks. Residues surrounding the structural Zn-coordination sites, W41, R62, and W66, are shown as sticks.



(C) Three possible docking modes of ampicillin onto the  $\text{Zn}_8^{\text{A104/G57}}\text{AB}_3$  catalytic sites as calculated with AutoDock. Surface representation of  $\text{Zn}_8^{\text{A104/G57}}\text{AB}_3$ . Structurally disordered loops are displayed as yellow ribbons. Potential substrate interaction sites, consisting of residues 58-60 and 104-105, are colored in blue. The ampicillin molecule is shown as sticks. The Zn center and the coordinated solvent molecule are depicted as navy and red spheres, respectively. The distances between the Zn-bound water molecule and the carbon of the  $\beta$ -lactam ring for each conformations are shown.

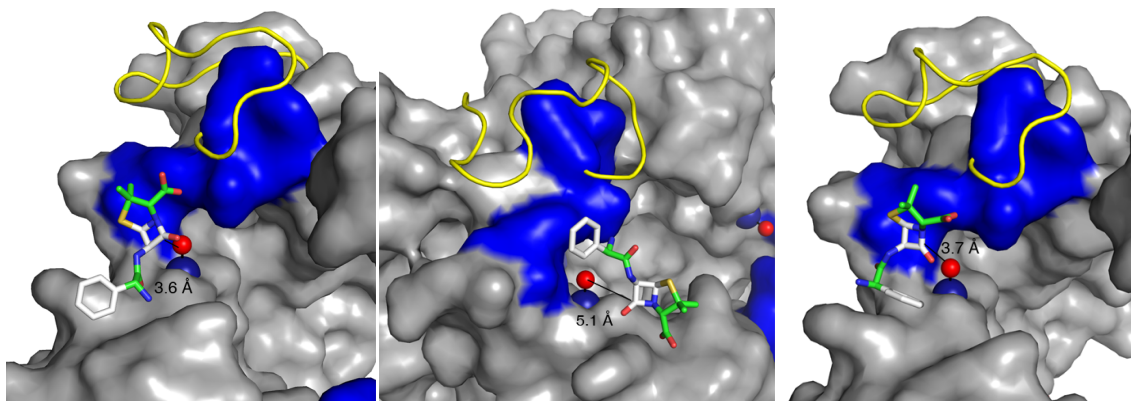


**Fig. S16.** Fluorescence emission spectra of 1-anilinonaphthalene-8-sulfonate (ANS) in the absence and presence of Zn-complexed proteins,  $\text{Zn}_4^{\text{C96}}\text{RIDC1}_4$ ,  $\text{Zn}_8\text{:AB3}_4$ , and  $\text{Zn}_8^{\text{A104/G57}}\text{AB3}_4$ .

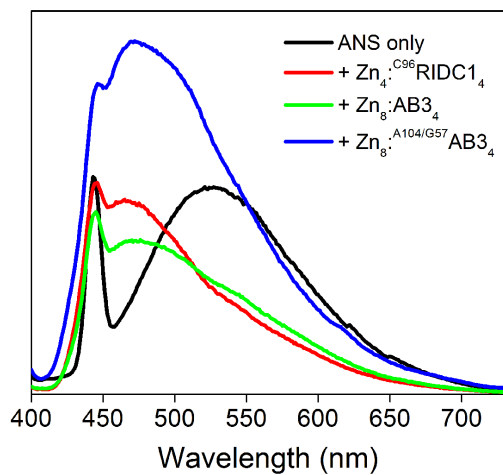
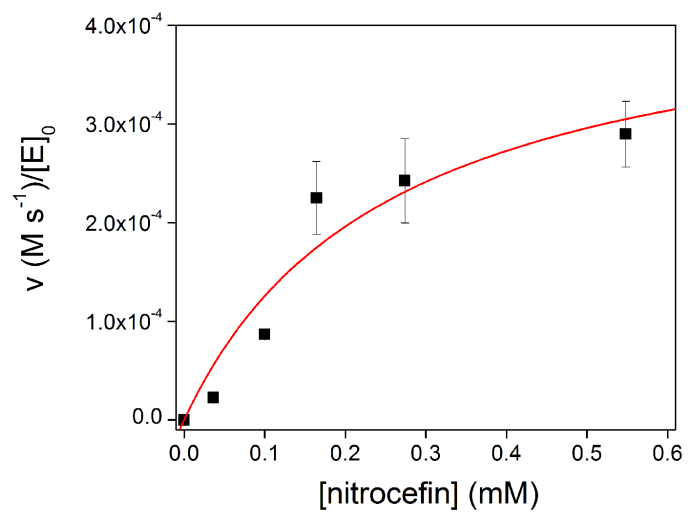


**Fig. S17.** Nitrocefin hydrolysis activity of  $\text{Zn}_8^{\text{A104/G57}}\text{AB3}_4$ .

(A) Michaelis-Menten kinetics.



(B) Measurement of uncatalyzed rate of nitrocefin hydrolysis in buffer solution.

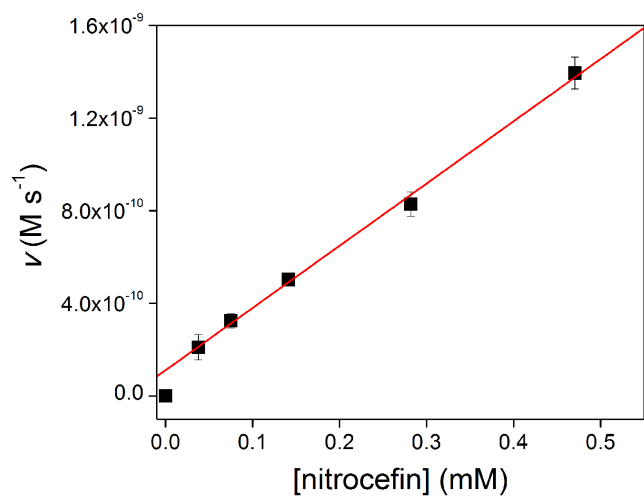


**Table S1.** Triads of potential Zn-binding residues on Zn<sub>4</sub>:<sup>C96</sup>RIDC1<sub>4</sub>. The triad variants prepared for this study are shown in bold with their abbreviated names in parentheses.

	Ligand, A	Ligand, B	Amino acid combination
A-set	89/93	100	<b>H/H/H (AB1)</b> E/H/H <b>H/E/H (AB4)</b> H/H/E
B-set	86/89	104	H/H/H E/H/H H/E/H H/H/E
C-set	86	100/104	H/H/H E/H/H H/E/H H/H/E
D-set	89	100/104	<b>H/H/H (AB2)</b> E/H/H H/E/H H/H/E
E-set	86/89	100	H/H/H <b>E/H/H (AB3)</b> H/E/H H/H/E

**Table S2.** DNA primers used in this study for site-directed mutagenesis.

Triad mutants	Mutations from <sup>96</sup> CRIDC-1	Primers
AB1 (H89/H93/H100)	A89H/Q93H  A100H	5'-GCGCAGCATGCTGCAGAGCATCTGAAATG-3' 5'-CATTTTCAGATGCTCTGCAGCATGCTGCGC-3' 5'-CCTGCAACCATTGCCACCAGAAGTATCG-3' 5'-CGATACTTCTGGTGGCAATGGTTGCAGG-3'
AB2 (H89/H100/H104)	E86D/A89H  A100H/K104H	5'-GTAAAAGATGCGCAGCATGCTGCAGCAAC-3' 5'-GTTGCTCTGCAGCGTACTGCGCATCTTTTAC-3' 5'-CAACCATTGCCACCAGCATTATCG-3' 5'-CGATAATGCTGGTGGCAATGGTTG-3'
AB3 (E86/H89/H100)	A89H  A100H	5'-GAAGCGCAGCATGCTGCAGAGCAACTG-3' 5'-CAGTTGCTCTGCAGCATGCTGCGCTTC-3' 5'-CCTGCAACCATTGCCACCAGAAGTATCG-3' 5'-CGATACTTCTGGTGGCAATGGTTGCAGG-3'
AB4 (H89/E93/H100)	A89H/Q93E  A100H  E86D	5'-GCGCAGCATGCTGCAGAGGAACTGAAATG-3' 5'-CATTTTCAGTTCCTCTGCAGCATGCTGCGC-3' 5'-CCTGCAACCATTGCCACCAGAAGTATCG-3' 5'-CGATACTTCTGGTGGCAATGGTTGCAGG-3' 5'-GTAAAAGATGCGCAGCATGCTGCAGCAAC-3' 5'-GTTGCTCTGCAGCATGCTGCGCATCTTTTAC-3'
AB3+K104A: <sup>A104</sup> AB3	K104A	5'-CCATTGCCACCAGGCGTATCGTTAATTCCTC-3' 5'-GAGGAATTAACGATACGCCTGGTGGCAATGG-3'

**Table S3.** Crystallographic data collection and refinement statistics (\*denotes highest resolution shell).

Protein	AB3	<sup>AI04/G57</sup> AB3
Data collection location	SSRL BL9-2	SSRL BL 14-1
Unit cell dimensions	54.8 × 54.8 × 237.8 $\alpha = \beta = 90^\circ, \gamma = 120^\circ$	71.3 × 92.2 × 98.6 $\alpha = \beta = \gamma = 90^\circ$
Symmetry group	<i>P6<sub>1</sub></i>	<i>F222</i>
Resolution (Å)	47.565- 2.50	35.66-2.80
X-ray wavelength (Å)	0.98	0.98
Number of unique reflections	13979	4159
Redundancy	9.0 (8.8)	4.3 (4.5)
Completeness (%)*	99.9 (100)	98.9 (100)
$\langle I / \sigma I \rangle$ *	15.2 (4.3)	22.2 (8.1)
$R_{\text{symm}}$ * (%)	7.7 (44.0)	4.8 (16.8)
$R_{\text{work}}/R_{\text{free}}$ (%)	23.8/29.6	24.5/28.9
Number of atoms	3524	954
Protein	3306	818
Ligands/ions	180	49
Water	38	87
B-factors (Å <sup>2</sup> )		
Protein		
Chain A	59.1	64.6
Chain B	65.7	
Chain C	64.4	
Chain D	90.5	
Ligands/ions	71.8	63.7
Water	52.4	56.3
R.m.s deviations		
Bond lengths (Å)	0.0049	0.0058
Bond angles (°)	0.9345	0.9361
PDB accession code	4U9D	4U9E

**Table S4.** Previously published pNPA hydrolysis activities of various proteinaceous and non-proteinaceous catalysts for comparison.

Catalyst/Enzyme	p <i>K</i> <sub>a</sub>	pH	<i>k</i> <sub>cat</sub> / <i>K</i> <sub>M</sub> (s <sup>-1</sup> M <sup>-1</sup> )	<i>k</i> <sub>2</sub> (s <sup>-1</sup> M <sup>-1</sup> )	Ref
CAI	7.3	9.0	370	-	(51)
CAII	6.8	9.0	2320	-	(51)
[12]aneN <sub>3</sub>	7.3	8.2	-	0.041	(52)
[12]aneN <sub>4</sub>	7.9	9.3	-	0.1	(25)
[15]aneN <sub>3</sub> O <sub>2</sub>	8.8		-	0.6 <sup>†</sup>	(53)
[12]aneN <sub>4</sub> hexadecyl derivative	7.56	10.5	-	5	(54)
PZD2		7.0	2.7	-	(55)
tris(4,5-di- <i>n</i> -propyl-2-imidazolyl) phosphine	8.7		-	0.86	(56)
[Hg(II)] <sub>s</sub> [Zn(II)(OH <sup>-</sup> ) <sub>3</sub> ]N(TRIL9CL23H) <sub>3</sub>	8.8	9.5	23.3(3)	-	(13)
		9.0	17.6(3)	-	
[Zn(II)]N(TRIL23H) <sub>3</sub> <sup>2+</sup>	9.0	9.0	14.1(3)	-	(13)
[Hg(II)] <sub>s</sub> [Zn(II)(OH <sup>-</sup> ) <sub>3</sub> ]N(CSL9PenL23H) <sub>3</sub> N <sup>+</sup>	nd	9.5	20(2)	-	(13)
MID1-zinc	8.2	9.0	660	-	(18)
Ac-IHIHIQI-CONH <sub>2</sub>	9.3	8.0 10.3	62 360	-	(26)
<sup>A104</sup> AB3 ( <sup>C96</sup> RIDC1 E86/H89/H100/A104)	9.0(2)	9.0 10.0	32(8) 120(20)	-	This work

<sup>†</sup>This value is from pH-dependent data.

**Table S5.** Dissociation constants for the Zn complexes of <sup>A104/G57</sup>AB3 and <sup>A104/T105</sup>AB3 variants. The values are the averages of two independent titrations. For representative titrations, see Fig. S6 and Fig. S11.

Proteins	$K_{d,1}$ (nM)	$K_{d,2}$ ( $\mu$ M)
<sup>A104</sup> AB3	6.7 (0.5)	0.40 (0.19)
<sup>A104/G57</sup> AB3	14 (10)	0.39 (0.24)
<sup>A104/T105</sup> AB3	36 (2)	1.62 (0.06)

## References and Notes

1. G. Kiss, N. Çelebi-Ölçüm, R. Moretti, D. Baker, K. N. Houk, Computational Enzyme Design. *Angew. Chem. Int. Ed.* **52**, 5700–5725 (2013). [doi:10.1002/anie.201204077](https://doi.org/10.1002/anie.201204077)
2. H. Kries, R. Blomberg, D. Hilvert, De novo enzymes by computational design. *Curr. Opin. Chem. Biol.* **17**, 221–228 (2013). [Medline doi:10.1016/j.cbpa.2013.02.012](https://pubmed.ncbi.nlm.nih.gov/23711112/)
3. R. Sterner, B. Höcker, Catalytic versatility, stability, and evolution of the (betaalpha)<sub>8</sub>-barrel enzyme fold. *Chem. Rev.* **105**, 4038–4055 (2005). [Medline doi:10.1021/cr030191z](https://pubmed.ncbi.nlm.nih.gov/15611112/)
4. M. Nardini, B. W. Dijkstra, Alpha/beta hydrolase fold enzymes: The family keeps growing. *Curr. Opin. Struct. Biol.* **9**, 732–737 (1999). [Medline doi:10.1016/S0959-440X\(99\)00037-8](https://pubmed.ncbi.nlm.nih.gov/10551112/)
5. H.-S. Park, S. H. Nam, J. K. Lee, C. N. Yoon, B. Mannervik, S. J. Benkovic, H. S. Kim, Design and evolution of new catalytic activity with an existing protein scaffold. *Science* **311**, 535–538 (2006). [Medline doi:10.1126/science.1118953](https://pubmed.ncbi.nlm.nih.gov/16611112/)
6. H. K. Privett, G. Kiss, T. M. Lee, R. Blomberg, R. A. Chica, L. M. Thomas, D. Hilvert, K. N. Houk, S. L. Mayo, Iterative approach to computational enzyme design. *Proc. Natl. Acad. Sci. U.S.A.* **109**, 3790–3795 (2012). [Medline doi:10.1073/pnas.1118082108](https://pubmed.ncbi.nlm.nih.gov/22111112/)
7. S. D. Khare, Y. Kipnis, P. Greisen Jr., R. Takeuchi, Y. Ashani, M. Goldsmith, Y. Song, J. L. Gallaher, I. Silman, H. Leader, J. L. Sussman, B. L. Stoddard, D. S. Tawfik, D. Baker, Computational redesign of a mononuclear zinc metalloenzyme for organophosphate hydrolysis. *Nat. Chem. Biol.* **8**, 294–300 (2012). [Medline doi:10.1038/nchembio.777](https://pubmed.ncbi.nlm.nih.gov/22111112/)
8. L. Giger, S. Caner, R. Obexer, P. Kast, D. Baker, N. Ban, D. Hilvert, Evolution of a designed retro-aldolase leads to complete active site remodeling. *Nat. Chem. Biol.* **9**, 494–498 (2013). [Medline doi:10.1038/nchembio.1276](https://pubmed.ncbi.nlm.nih.gov/23111112/)
9. N. Yeung, Y. W. Lin, Y. G. Gao, X. Zhao, B. S. Russell, L. Lei, K. D. Miner, H. Robinson, Y. Lu, Rational design of a structural and functional nitric oxide reductase. *Nature* **462**, 1079–1082 (2009). [Medline doi:10.1038/nature08620](https://pubmed.ncbi.nlm.nih.gov/19111112/)
10. P. S. Coelho, E. M. Brustad, A. Kannan, F. H. Arnold, Olefin cyclopropanation via carbene transfer catalyzed by engineered cytochrome P450 enzymes. *Science* **339**, 307–310 (2013). [Medline doi:10.1126/science.1231434](https://pubmed.ncbi.nlm.nih.gov/23111112/)
11. T. K. Hyster, L. Knörr, T. R. Ward, T. Rovis, Biotinylated Rh(III) complexes in engineered streptavidin for accelerated asymmetric C-H activation. *Science* **338**, 500–503 (2012). [Medline doi:10.1126/science.1226132](https://pubmed.ncbi.nlm.nih.gov/22111112/)
12. M. Faiella, C. Andreozzi, R. T. de Rosales, V. Pavone, O. Maglio, F. Nastri, W. F. DeGrado, A. Lombardi, An artificial di-iron oxo-protein with phenol oxidase activity. *Nat. Chem. Biol.* **5**, 882–884 (2009). [Medline doi:10.1038/nchembio.257](https://pubmed.ncbi.nlm.nih.gov/19111112/)
13. M. L. Zastrow, A. F. Peacock, J. A. Stuckey, V. L. Pecoraro, Hydrolytic catalysis and structural stabilization in a designed metalloprotein. *Nat. Chem.* **4**, 118–123 (2012). [Medline doi:10.1038/nchem.1201](https://pubmed.ncbi.nlm.nih.gov/22111112/)
14. M. H. Ali, B. Imperiali, Protein oligomerization: How and why. *Bioorg. Med. Chem.* **13**, 5013–5020 (2005). [Medline doi:10.1016/j.bmc.2005.05.037](https://pubmed.ncbi.nlm.nih.gov/16111112/)

15. E. N. Salgado, R. J. Radford, F. A. Tezcan, Metal-directed protein self-assembly. *Acc. Chem. Res.* **43**, 661–672 (2010). [Medline doi:10.1021/ar900273t](#)
16. B. S. Der, M. Machius, M. J. Miley, J. L. Mills, T. Szyperski, B. Kuhlman, Metal-mediated affinity and orientation specificity in a computationally designed protein homodimer. *J. Am. Chem. Soc.* **134**, 375–385 (2012). [Medline doi:10.1021/ja208015j](#)
17. W. J. Song, P. A. Sontz, X. I. Ambroggio, F. A. Tezcan, Metals in protein-protein interfaces. *Annu. Rev. Biophys.* **43**, 409–431 (2014). [Medline doi:10.1146/annurev-biophys-051013-023038](#)
18. B. S. Der, D. R. Edwards, B. Kuhlman, Catalysis by a de novo zinc-mediated protein interface: Implications for natural enzyme evolution and rational enzyme engineering. *Biochemistry* **51**, 3933–3940 (2012). [Medline doi:10.1021/bi201881p](#)
19. K. Channon, E. H. Bromley, D. N. Woolfson, Synthetic biology through biomolecular design and engineering. *Curr. Opin. Struct. Biol.* **18**, 491–498 (2008). [Medline doi:10.1016/j.sbi.2008.06.006](#)
20. J. F. Fisher, S. O. Meroueh, S. Mobashery, Bacterial resistance to beta-lactam antibiotics: Compelling opportunism, compelling opportunity. *Chem. Rev.* **105**, 395–424 (2005). [Medline doi:10.1021/cr030102i](#)
21. M. W. Crowder, J. Spencer, A. J. Vila, Metallo-beta-lactamases: Novel weaponry for antibiotic resistance in bacteria. *Acc. Chem. Res.* **39**, 721–728 (2006). [Medline doi:10.1021/ar0400241](#)
22. J. Faraone-Mennella, F. A. Tezcan, H. B. Gray, J. R. Winkler, Stability and folding kinetics of structurally characterized cytochrome c-b562. *Biochemistry* **45**, 10504–10511 (2006). [Medline doi:10.1021/bi060242x](#)
23. E. N. Salgado, J. Faraone-Mennella, F. A. Tezcan, Controlling protein-protein interactions through metal coordination: Assembly of a 16-helix bundle protein. *J. Am. Chem. Soc.* **129**, 13374–13375 (2007). [Medline doi:10.1021/ja075261o](#)
24. J. D. Brodin, A. Medina-Morales, T. Ni, E. N. Salgado, X. I. Ambroggio, F. A. Tezcan, Evolution of metal selectivity in templated protein interfaces. *J. Am. Chem. Soc.* **132**, 8610–8617 (2010). [Medline doi:10.1021/ja910844n](#)
25. T. Koike, M. Takamura, E. Kimura, Role of zinc(II) in  $\beta$ -lactamase II: A model study with a zinc(II)-macrocyclic tetraamine (1,4,7,10-tetraazacyclododecane, cyclen) complex. *J. Am. Chem. Soc.* **116**, 8443–8449 (1994). [doi:10.1021/ja00098a002](#)
26. C. M. Rufo, Y. S. Moroz, O. V. Moroz, J. Stöhr, T. A. Smith, X. Hu, W. F. DeGrado, I. V. Korendovych, Short peptides self-assemble to produce catalytic amyloids. *Nat. Chem.* **6**, 303–309 (2014). [Medline doi:10.1038/nchem.1894](#)
27. A. Medina-Morales, A. Perez, J. D. Brodin, F. A. Tezcan, In vitro and cellular self-assembly of a Zn-binding protein cryptand via templated disulfide bonds. *J. Am. Chem. Soc.* **135**, 12013–12022 (2013). [Medline doi:10.1021/ja405318d](#)
28. W. Maret, Y. Li, Coordination dynamics of zinc in proteins. *Chem. Rev.* **109**, 4682–4707 (2009). [Medline doi:10.1021/cr800556u](#)

29. M. T. Reetz, J. D. Carballeira, Iterative saturation mutagenesis (ISM) for rapid directed evolution of functional enzymes. *Nat. Protoc.* **2**, 891–903 (2007). [Medline](#) [doi:10.1038/nprot.2007.72](https://doi.org/10.1038/nprot.2007.72)
30. N. V. Kaminskaia, C. He, S. J. Lippard, Reactivity of mu-hydroxodizinc(II) centers in enzymatic catalysis through model studies. *Inorg. Chem.* **39**, 3365–3373 (2000). [Medline](#) [doi:10.1021/ic000169d](https://doi.org/10.1021/ic000169d)
31. M. Vanhove, M. Zakhem, B. Devreese, N. Franceschini, C. Anne, C. Bebrone, G. Amicosante, G. M. Rossolini, J. Van Beumen, J. M. Frère, M. Galleni, Role of Cys221 and Asn116 in the zinc-binding sites of the *Aeromonas hydrophila* metallo- $\beta$ -lactamase. *CMLS. Cell. Mol. Life Sci.* **60**, 2501–2509 (2003). [Medline](#) [doi:10.1007/s00018-003-3092-x](https://doi.org/10.1007/s00018-003-3092-x)
32. S. D. B. Scrofan, J. Chung, J. J. A. Huntley, S. J. Benkovic, P. E. Wright, H. J. Dyson, NMR characterization of the metallo- $\beta$ -lactamase from *Bacteroides fragilis* and its interaction with a tight-binding inhibitor: Role of an active-site loop. *Biochemistry* **38**, 14507–14514 (1999). [Medline](#) [doi:10.1021/bi990986t](https://doi.org/10.1021/bi990986t)
33. P. E. Tomatis, S. M. Fabiane, F. Simona, P. Carloni, B. J. Sutton, A. J. Vila, Adaptive protein evolution grants organismal fitness by improving catalysis and flexibility. *Proc. Natl. Acad. Sci. U.S.A.* **105**, 20605–20610 (2008). [Medline](#) [doi:10.1073/pnas.0807989106](https://doi.org/10.1073/pnas.0807989106)
34. D. S. Tawfik, Biochemistry. Loop grafting and the origins of enzyme species. *Science* **311**, 475–476 (2006). [Medline](#) [doi:10.1126/science.1123883](https://doi.org/10.1126/science.1123883)
35. N. Tokuriki, D. S. Tawfik, Protein dynamism and evolvability. *Science* **324**, 203–207 (2009). [Medline](#) [doi:10.1126/science.1169375](https://doi.org/10.1126/science.1169375)
36. M. Braun, L. Thöny-Meyer, Biosynthesis of artificial microperoxidases by exploiting the secretion and cytochrome c maturation apparatuses of *Escherichia coli*. *Proc. Natl. Acad. Sci. U.S.A.* **101**, 12830–12835 (2004). [Medline](#) [doi:10.1073/pnas.0402435101](https://doi.org/10.1073/pnas.0402435101)
37. P. Kuzmič, Program DYNAFIT for the analysis of enzyme kinetic data: Application to HIV proteinase. *Anal. Biochem.* **237**, 260–273 (1996). [Medline](#) [doi:10.1006/abio.1996.0238](https://doi.org/10.1006/abio.1996.0238)
38. P. Schuck, Size-distribution analysis of macromolecules by sedimentation velocity ultracentrifugation and lamm equation modeling. *Biophys. J.* **78**, 1606–1619 (2000). [Medline](#) [doi:10.1016/S0006-3495\(00\)76713-0](https://doi.org/10.1016/S0006-3495(00)76713-0)
39. Collaborative Computational Project, Number 4, The CCP4 suite: Programs for protein crystallography. *Acta Crystallogr. D Biol. Crystallogr.* **50**, 760–763 (1994). [Medline](#) [doi:10.1107/S0907444994003112](https://doi.org/10.1107/S0907444994003112)
40. A. J. McCoy, R. W. Grosse-Kunstleve, P. D. Adams, M. D. Winn, L. C. Storoni, R. J. Read, *Phaser* crystallographic software. *J. Appl. Cryst.* **40**, 658–674 (2007). [doi:10.1107/S0021889807021206](https://doi.org/10.1107/S0021889807021206)
41. G. N. Murshudov, A. A. Vagin, E. J. Dodson, Refinement of macromolecular structures by the maximum-likelihood method. *Acta Crystallogr. D Biol. Crystallogr.* **53**, 240–255 (1997). [doi:10.1107/S0907444996012255](https://doi.org/10.1107/S0907444996012255)

42. R. A. Laskowski, M. W. MacArthur, D. S. Moss, J. M. Thornton, PROCHECK: A program to check the stereochemical quality of protein structures. *J. Appl. Cryst.* **26**, 283–291 (1993). [doi:10.1107/S0021889892009944](https://doi.org/10.1107/S0021889892009944)
43. A. Nomura, Y. Sugiura, Hydrolytic reaction by zinc finger mutant peptides: Successful redesign of structural zinc sites into catalytic zinc sites. *Inorg. Chem.* **43**, 1708–1713 (2004). [Medline doi:10.1021/ic034931y](https://pubmed.ncbi.nlm.nih.gov/15011211/)
44. Z. Wang, W. Fast, S. J. Benkovic, On the mechanism of the metallo-beta-lactamase from *Bacteroides fragilis*. *Biochemistry* **38**, 10013–10023 (1999). [Medline doi:10.1021/bi990356r](https://pubmed.ncbi.nlm.nih.gov/10511211/)
45. N. G. Nossal, L. A. Heppel, The release of enzymes by osmotic shock from *Escherichia coli* in exponential phase. *J. Biol. Chem.* **241**, 3055–3062 (1966). [Medline](https://pubmed.ncbi.nlm.nih.gov/13611211/)
46. E. N. Salgado, X. I. Ambroggio, J. D. Brodin, R. A. Lewis, B. Kuhlman, F. A. Tezcan, Metal templated design of protein interfaces. *Proc. Natl. Acad. Sci. U.S.A.* **107**, 1827–1832 (2010). [Medline doi:10.1073/pnas.0906852107](https://pubmed.ncbi.nlm.nih.gov/20611211/)
47. A. W. Schüttelkopf, D. M. van Aalten, PRODRG: A tool for high-throughput crystallography of protein-ligand complexes. *Acta Crystallogr. D Biol. Crystallogr.* **60**, 1355–1363 (2004). [Medline doi:10.1107/S0907444904011679](https://pubmed.ncbi.nlm.nih.gov/15111211/)
48. O. Trott, A. J. Olson, AutoDock Vina: Improving the speed and accuracy of docking with a new scoring function, efficient optimization, and multithreading. *J. Comput. Chem.* **31**, 455–461 (2010). [Medline](https://pubmed.ncbi.nlm.nih.gov/20511211/)
49. X.-C. Yu, H. W. Strobel, Interactions of 8-anilino-1-naphthalenesulfonic acid (ANS) and cytochrome P450 2B1: Role of ANS as an effector as well as a reporter group. *Mol. Cell. Biochem.* **162**, 89–95 (1996). [Medline doi:10.1007/BF00227534](https://pubmed.ncbi.nlm.nih.gov/9011211/)
50. G. Weber, L. B. Young, Fragmentation of bovine serum albumin by pepsin. I. The origin of the acid expansion of the albumin molecule. *J. Biol. Chem.* **239**, 1415–1423 (1964). [Medline](https://pubmed.ncbi.nlm.nih.gov/13611211/)
51. J. A. Verpoorte, S. Mehta, J. T. Edsall, Esterase activities of human carbonic anhydrases B and C. *J. Biol. Chem.* **242**, 4221–4229 (1967). [Medline](https://pubmed.ncbi.nlm.nih.gov/13611211/)
52. E. Kimura, T. Shiota, T. Koike, M. Shiro, M. Kodama, A zinc(II) complex of 1,5,9-triazacyclododecane ([12]aneN<sub>3</sub>) as a model for carbonic anhydrase. *J. Am. Chem. Soc.* **112**, 5805–5811 (1990). [doi:10.1021/ja00171a020](https://pubmed.ncbi.nlm.nih.gov/19011211/)
53. C. Bazzicalupi, A. Bencini, A. Bianchi, V. Fusi, C. Giorgi, P. Paoletti, B. Valtancoli, D. Zanchi, Carboxy and phosphate esters cleavage with mono- and dinuclear zinc(ii) macrocyclic complexes in aqueous solution. Crystal structure of [Zn<sub>2</sub>L1(μ-PP)<sub>2</sub>(MeOH)<sub>2</sub>](ClO<sub>4</sub>)<sub>2</sub> (L1 = [30]aneN<sub>6</sub>O<sub>4</sub>, PP<sup>-</sup> = diphenyl phosphate). *Inorg. Chem.* **36**, 2784–2790 (1997). [Medline doi:10.1021/ic961521j](https://pubmed.ncbi.nlm.nih.gov/15011211/)
54. E. Kimura, H. Hashimoto, T. Koike, Hydrolysis of lipophilic esters catalyzed by a zinc(II) complex of a long alkyl-pendant macrocyclic tetraamine in micellar solution. *J. Am. Chem. Soc.* **118**, 10963–10970 (1996). [doi:10.1021/ja961789+](https://pubmed.ncbi.nlm.nih.gov/14011211/)
55. D. N. Bolon, S. L. Mayo, Enzyme-like proteins by computational design. *Proc. Natl. Acad. Sci. U.S.A.* **98**, 14274–14279 (2001). [Medline doi:10.1073/pnas.251555398](https://pubmed.ncbi.nlm.nih.gov/11811211/)

56. T. B. Koerner, R. S. Brown, The hydrolysis of an activated ester by a tris(4,5-di- *n*- propyl-2-imidazolyl)phosphine-Zn<sup>2+</sup> complex in neutral micellar medium as a model for carbonic anhydrase. *Can. J. Chem.* **80**, 183–191 (2002). [doi:10.1139/v02-001](https://doi.org/10.1139/v02-001)